Published in final edited form as:
J Am Chem Soc. 2011 December 28; 133(51): 20878–20889. doi:10.1021/ja2077476.

A Comparison of Two Yeast MnSODs: Mitochondrial *Saccharomyces cerevisiae* versus Cytosolic *Candida albicans*

Yuewei Sheng[†], **Troy A. Stich**[‡], **Kevin Barnese**[†], **Edith B. Gralla**[†], **Duilio Cascio**[|], **R. David Britt**[‡], **Diane E. Cabelli**[*,§], and **Joan Selverstone Valentine**[*,†,⊥]

[†]Department of Chemistry and Biochemistry, University of California Los Angeles, 420 Westwood Plaza, Los Angeles, California 90095, USA

[|]Department of Energy-Institute for Genomics and Proteomics, University of California Los Angeles, 420 Westwood Plaza, Los Angeles, California 90095, USA

[‡]Department of Chemistry, University of California Davis, One Shields Avenue, Davis, California 95616, USA

[§]Chemistry Department, Brookhaven National Laboratory, Upton, NY 11973, USA

[⊥]Department of Bioinspired Sciences, Ewha Womans University, Seoul 120-750, Republic of Korea

Abstract

Human MnSOD is significantly more product-inhibited than bacterial MnSODs at high concentrations of superoxide (O_2^-). This behavior limits the amount of H_2O_2 produced at high [O_2^-]; its desirability can be explained by the multiple roles of H_2O_2 in mammalian cells, particularly its role in signaling. To investigate the mechanism of product inhibition in MnSOD, two yeast MnSODs, one from *Saccharomyces cerevisiae* mitochondria (*Sc*MnSOD) and the other from *Candida albicans* cytosol (*Ca*MnSODc), were isolated and characterized. *Sc*MnSOD and *Ca*MnSODc are similar in catalytic kinetics, spectroscopy and redox chemistry, and they both rest predominantly in the reduced state (unlike most other MnSODs). At high [O_2^-] the dismutation efficiencies of the yeast MnSODs surpass those of human and bacterial MnSODs, due to very low level of product inhibition. Optical and parallel-mode electron paramagnetic resonance (EPR) spectra suggest the presence of two Mn^{3+} species in yeast Mn^{3+}SODs, including the well-characterized 5-coordinate Mn^{3+} species and a 6-coordinate L-Mn^{3+} species with hydroxide as the putative sixth ligand (L). The first and second coordination spheres of *Sc*MnSOD are more similar to bacterial than to human MnSOD. Gln154, an H-bond donor to the Mn-coordinated solvent molecule, is slightly further away from Mn in yeast MnSODs, which may result in their unusual resting state. Mechanistically, the high efficiency of yeast MnSODs could be ascribed to putative translocation of an outer-sphere solvent molecule, which could destabilize the inhibited complex and enhance proton transfer from protein to peroxide. Our studies on yeast MnSODs indicate the unique nature of human MnSOD in that it predominantly undergoes the inhibited pathway at high [O_2^-].

[*]**Corresponding Author**: jsv@chem.ucla.edu; cabelli@bnl.gov .

ASSOCIATED CONTENT

Supporting Information. Crystallization conditions, pulse radiolysis, optical and EPR spectra, crystallography information and active site bond distances. This material is available free of charge via the Internet at http://pubs.acs.org.

INTRODUCTION

Superoxide dismutases (SODs) are enzymes that function to convert the superoxide (O_2^-) anion to dioxygen and hydrogen peroxide (H_2O_2) catalytically via sequential reduction and oxidation of a metal cofactor at virtually diffusion-controlled rate constants (Scheme 1).

Manganese-containing superoxide dismutases (MnSODs) are found in a wide variety of species and, in these species, it can be localized either in the cytosol or the mitochondria or both. In bacteria, MnSOD is cytosolic while in yeast both mitochondrial and cytosolic forms exist. In mammalian cells it is mitochondrial. MnSOD catalyzes the disproportionation of O_2^- by a mechanism that distinguishes it from the other SODs in that it becomes a less effective antioxidant when O_2^- levels are high relative to enzyme concentration.[1] Specifically, human MnSOD[2] has been shown to be very inefficient at removal of high concentrations of O_2^- whereas the MnSOD from bacteria (*Escherichia coli*[2] and *Deinococcus radiodurans*[3]) and yeast (*Saccharomyces cerevisiae*)[4] are more efficient under the same conditions. It is this feature of differential efficiency at O_2^- removal that led to our interest in exploring the activity of MnSODs from different cellular sources and locations.

Efficient removal of high concentrations of O_2^- will, by necessity, produce high local concentrations of H_2O_2. H_2O_2 is a biologically important class of reactive oxygen species (ROS). It can be reduced to hydroxyl radical ($^{\bullet}OH$) through a Fenton-type reaction with a reduced metal ($M^{(n-1)+} + H_2O_2 \rightarrow M^{n+} + OH^- + {}^{\bullet}OH$), whose reaction with cellular components causes severe damage to lipids, proteins, and nucleotides. The oxidative damage caused both directly and indirectly by H_2O_2 is implicated in cancer and aging.[5,6] Besides its toxic effects, the roles of H_2O_2 in aiding phagocytes in the killing of ingested microorganisms as well as in some oxidative biosynthesis are well known.[7] In addition in recent years there is rising evidence of H_2O_2 functioning as a signaling agent in higher organisms.[7-11]

The mechanism by which MnSOD removes high O_2^- concentrations less efficiently than other SODs involves product inhibition. The overall reduction of O_2^- by an oxidized metal (Scheme 2), when carried out by Mn^{2+}SOD, occurs either through a pathway (reaction 2) where delivery of protons to the bound peroxo moiety is effectively instantaneous (an “outer-sphere” pathway), or through a pathway (reaction 3) where an identifiable transient is formed (an “inner-sphere” pathway), defined here as a “product-inhibited” complex that has been described as a side-on Mn(III)-peroxo species[12]. The inner-sphere pathway can become significant at high O_2^- concentrations and, if the dissociation of peroxide (k_4) is relatively slow, this can lead to reduced catalytic efficiency of MnSOD. The level of product inhibition is described by k_2/k_3, the gating ratio of the two pathways.

S. cerevisiae is an important single-cell model for studying human and other eukaryotic cells. Like human cells, it expresses a homotetrameric MnSOD in its mitochondria (*Sc*MnSOD), which shares sequence similarity with human MnSOD. To our surprise, our previous study showed *Sc*MnSOD to be the most efficient at removing high O_2^- concentrations, among MnSODs that have been characterized to date.[4] However, the origins of the low level of product inhibition are unclear.

S. cerevisiae and humans have a common cellular localization of their SODs. They both have MnSODs only in their mitochondrion and copper-zinc SODs (CuZnSOD) in their cytosol. In contrast, a closely related yeast *Candida albicans* expresses a MnSOD that lacks the mitochondrial leader sequence and is active in the cytosol (*Ca*MnSODc)* in addition to its mitochondrial *Ca*MnSOD and cytosolic *Ca*CuZnSOD. *Ca*MnSODc shares 70% sequence similarity with *Sc*MnSOD and has been proposed to be important for survival of *C. albicans*

in nutrient-limiting conditions.[13] Overexpression of *Ca*MnSODc has been shown to rescue the phenotypes of *S. cerevisiae* strain lacking the cytosolic CuZnSOD.[13]

In order to understand further the mechanism of product inhibition in MnSOD and its implication in H_2O_2 signaling in higher organisms, we isolated and characterized *Sc*MnSOD and *Ca*MnSODc. Herein we report the first comparison of the catalytic activity of the two yeast MnSODs, the crystal structures of their metal-binding sites, and their spectroscopic characterization. We discuss how these factors relate to the function of yeast MnSODs; we further compare human, bacterial, and yeast MnSODs; and we explore the implications with respect to the evolution of H_2O_2 signaling.

MATERIALS AND METHODS

DNA Manipulation of *Ca*MnSODc and Transformation into *S. cerevisiae*

The pVT102U-*Ca*MnSODc (with *URA*3 and *AMP* marker) vector containing the complete coding sequence of *Ca*MnSODc was generously provided by Prof. Bourbonnais.[13] Sequencing shows that it is an I169V mutant of the wild-type protein accidentally created during cloning. The primers 5′-GTTCCAATTATTGCC**A**TCGATGCTTGGGAA-C-3′ and 5′-GTTCCCAAGCATCGA**T**GGCAATAATTGGA-AC-3′ were used to create the wild-type cDNA (mutations are in bold type). The PCR products were transformed into *E. coli* DH5α strain and screened by ampicillin selection. The purified pVT102U-*Ca*MnSODc vector was transformed into *S. cerevisiae sod*2Δ strain (EG110; *Mat-alpha, ura3, leu2, trp1, his3, sod2::TRP1*).

Expression and Purification of *Sc*MnSOD and *Ca*MnSODc

Yeast cells carrying Yep352-*Sc*MnSOD[4] were grown in YPEG media (1% yeast extract, 2% peptone, 3% glycerol, 2% ethanol, pH 4) supplemented with 0.5 mM Mn(II) sulfate at 30 °C to O.D. > 20, and then harvested by centrifugation at 12,000 × g for 10 min. *Sc*MnSOD was-isolated as previously described.[4]

Yeast cells carrying pVT102U-*Ca*MnSODc were grown in YPD (1% yeast extract, 2% peptone, 2% dextrose, pH 4) media supplemented with 0.5 mM Mn(II) sulfate at 30 °C to O.D. > 10, and then harvested by centrifugation at 12,000 × g for 10 min. The procedures for isolation of *Ca*MnSODc and *Sc*MnSOD were the same[4] except that the procedures of the DE52 column were different. *Ca*MnSODc does not bind tightly to the DE52 resin while most other proteins in the crude extract do. The active fractions from the hydrophobic interaction column were pooled and dialyzed against water and then 5 mM potassium phosphate, pH 8 at 4 °C. The protein then was loaded on a DE52 column, washed with 2 column volumes of 5 mM potassium phosphate, pH 8. *Ca*MnSODc fell into the load and wash during the chromatography. The load and wash were combined, concentrated, and loaded onto a G300 gel filtration column.

Pulse Radiolysis

The pulse radiolysis experiments were carried out using the 2 MeV Van de Graaff accelerator at Brookhaven National Laboratory. Upon irradiation of water with a pulse of energetic electrons, hydrated electrons (e_{aq}^-), hydroxyl radicals ($^{\bullet}OH$) and, in lesser yield, hydrogen atoms ($H^{\bullet}$) are the primary radicals produced. Superoxide radical is then generated in air-saturated aqueous solution containing sodium formate through the following

*We have chosen for the sake of convenience to distinguish between cytosolic and mitochondrial MnSODs by adding a “c” to the MnSOD to indicate that it is a cytosolic enzyme. This distinction becomes important in those organisms (*C. albicans*) where MnSOD is found in both locations. This distinction is not relevant to human and *S. cerevisiae* as all of the MnSOD is mitochondrial.

reactions: $^{\bullet}OH + HCO_2^- \rightarrow H_2O + CO_2^{\bullet-}$, $O_2 + CO_2^{\bullet-} \rightarrow O_2^{\bullet-} + CO_2$, $e_{aq}^- + O_2 \rightarrow O_2^{\bullet-}$, $H^{\bullet} + O_2 \rightarrow HO_2^{\bullet}$.

The experiments to measure catalytic rates were carried out using two methodologies. One set of studies involved oxidizing the resting enzyme with substoichiometric quantities of O_2^- and following the appearance of Mn^{3+}SOD which has an absorbance band at around 480 nm (extinction coefficient ≈ 800 $M^{-1}cm^{-1}$). The rate of reaction 2 (k_2) was determined by fitting the resultant time trace of Mn^{3+} growth to a first-order reaction. In this set of experiments, 2:1 [H_2O_2]:[MnSOD] was added as previous studies had shown that H_2O_2 effectively reduces Mn^{3+}SOD to Mn^{2+}SOD. The other method involved following the decay of various concentrations of O_2^- at 260 nm using a 1:1 to 1:50 ratio of [MnSOD]:[O_2^-]. Here, all the rate constants except k_2 were calculated by fitting the data obtained to a mechanism described in Scheme 2 using the Chemical Kinetics program in PRWIN[14].

All pulse radiolysis samples were prepared in 10 mM potassium phosphate, 10 mM sodium formate and 10 or 100 μM EDTA at 25 °C. All MnSOD concentrations were taken as the ICP-measured concentration of manganese in the sample. As all of the manganese concentrations were less than the corresponding protein concentrations, we assumed that all of the manganese was bound. This had the advantage of allowing direct comparison of activity of a tetrametric and a dimeric enzyme as everything is normalized to a monomeric unit. However, it also assumes no cooperativity between metal sites. The pH of the buffer was adjusted using ultrapure (Baker Ultrex) sodium hydroxide and sulphuric acid as needed.

EPR Spectroscopy

X-band (9.47 GHz) perpendicular-polarization ($B_0 \perp B_1$) continuous-wave electron paramagnetic resonance (CW EPR) spectra were recorded using a Bruker ECS106 spectrometer equipped with a TE102 cavity (ER3902ST). Parallel-polarization ($B_0 \parallel B_1$) data were acquired using a dual-mode cavity (ER 4116DM) operating at 9.39 GHz. Cryogenic temperatures were achieved and controlled using an Oxford Instruments ESR900 liquid helium cryostat in conjunction with an Oxford Instruments ITC503 temperature and gas flow controller. Spectral simulations were performed in MatLab using EasySpin 3.1.[15,16]

Crystallization of *Sc*MnSOD and *Ca*MnSODc

The apoprotein of *Sc*MnSOD aggregates after the native protein is heated at 70 °C in MOPS, while the metallated *Sc*MnSOD stays folded in solution. Fully metallated *Sc*MnSOD was obtained by heating as-isolated protein (20 mM MOPS, pH 7) at 70 °C for 1 hr and removing aggregated protein by centrifugation. The reductive methylation of lysine residues of *Sc*MnSOD was carried out as described, in order to improve the diffraction of protein crystals.[17] The activity of native and methylated *Sc*MnSOD is similar in SOD activity assay.[18] All the free amino groups of lysine residues and the N-terminal were methylated as confirmed by mass spectrometry (Figure S1).

Methylated *Sc*MnSOD was crystallized by hanging-drop vapor diffusion at 4 °C against a well solution of 0.2 M sodium malonate (pH 7) in 20% (w/v) polyethylene glycol 3,350 with a protein concentration of 7 mg/mL. Native *Ca*MnSODc was crystallized by hanging-drop vapor diffusion at 4 °C against a solution of 0.1 M magnesium chloride, 0.1 M sodium chloride and 0.1 M tri-sodium citrate (pH 5.5) in 30% (w/v) polyethylene glycol 400 with a protein concentration of 7 mg/mL. *Sc*MnSOD and *Ca*MnSODc crystals were cryoprotected in mother liquor solution containing 30% glycerol and flash frozen in liquid nitrogen prior to data collection.

Crystallography: Data Collection and Refinement

All data was collected at 100K at the UCLA X-ray diffraction facility, using a Rigaku FRE+ generator and a Rigaku HTC detector. All data was processed using DENZO and SCALEPACK.[19] *Sc*MnSOD was phased by molecular replacement using human MnSOD Q143N mutant (1QNM). *Ca*MnSODc was phased by molecular replacement using *Sc*MnSOD (3LSU). All the molecular replacement was done using PHASER.[20] The models were built using COOT.[21] All model refinement was done using REFMAC[22] and PHENIX[23].

Coordinates and structure factors have been deposited in the PDB with accession numbers 3LSU for the *Sc*MnSOD structure and 3QVN for the *Ca*MnSODc structure.

Miscellaneous Methods

The metal contents of the purified proteins were determined by ICP-MS (Agilent 7500 series). UV-Visible absorption spectra were collected on a Shimadzu UV-2501 PC spectrophotometer.

The mass weight of the protein subunit was determined by an electrospray ionization mass spectrometry (ESI-MS) via a triple quadrupole instrument (API III, Applied Biosystems). An m/z 600–2,200 range was scanned (positive mode, orifice 90 V, 0.3 Da step size, 5.61 s/scan). Data were processed and analyzed using MacSpec 3.3, Hypermass and BioMultiview 1.3.1 software (Applied Biosystems).

The mass weight of the native protein was determined by a HPLC (Agilent 1200 series) fitted with a size exclusion col umn (Tosoh Bioscience, TSK gel G2000SW 7.5 mm ID × 30 cm) at a flow rate of 0.5 mL/min. The column was calibrated using five standards: bovine thyroglobulin (670 kDa), bovine γ-globulin (158 kDa), ovalbumin (44 kDa), horse myoglobin (17 kDa), and vitamin B12 (1.35 kDa).

RESULTS

Tetramer versus Dimer

*Ca*MnSODc was overexpressed and purified from *S. cerevisiae*, with 0.6 equiv of manganese per subunit as determined by ICP-MS. The subunit mass weight is 22.7 kDa as determined by ESI-MS. The purity was confirmed by SDS-PAGE gel (Figure S2). *Ca*MnSODc has been reported to be a homotetramer[13], but our investigation of the native protein using gel filtration chromatography indicates that its molecular weight in solution under our conditions is ~46 kDa, corresponding to a homodimer (Figure 1). It should be noted, however, that we found that *Ca*MnSODc crystallized as a tetramer under other conditions (see below). *Sc*MnSOD, in contrast to *Ca*MnSODc and analogous to the human MnSOD, is a homotetramer under our conditions, although the two yeast enzymes share great sequence similarity.

Kinetic Studies

Solutions containing 1 μM MnSOD at pH 7 were pulse irradiated and the disappearance of O_2^- was followed at 260 nm; see Figure 2. The traces we collected for both *Ca*MnSODc and *Sc*MnSOD were plotted along with previous data collected under identical conditions for MnSOD from human, *E. coli* and *D. radiodurans*.[2,3] When the O_2^- concentration was seven-fold excess over the enzyme, human MnSOD already showed a depressed activity, yet the O_2^- disappearance as a function of time was similar for the other four enzymes and could be fit to a first-order process (Figure 2A). When the ratio of [O_2^-]:MnSOD increased to 41, the five MnSODs displayed dramatically different efficiencies at removing O_2^-

(Figure 2B), which scale as *Ca*MnSODc > *Sc*MnSOD > *D. radiodurans* (*Dr*MnSOD) > *E. coli* (*Ec*MnSOD) > human MnSOD. For human and *E. coli* MnSOD, the O_2^- decay was characterized by a fast decrease, followed by a slow almost zero-order phase. It is the biphasic nature of the trace that suggests dismutation proceeded by a fast catalytic pathway and a slower, concomitant product-inhibited pathway. The gating values for these two enzymes are 1 and 5 respectively.[2] The trace obtained for the *Dr*MnSOD showed a much less distinct plateau region and fitting the data yielded a gating value of 12.[3] Our earlier study of the reaction of *Sc*MnSOD with high O_2^- concentrations led to a calculated gating value k_2/k_3 to be 16-20, indicating that the fast protonation pathway dominates.[4]

*Ca*MnSODc removes high concentrations of O_2^- even more efficiently than *Sc*MnSOD. Here, k_2 of *Ca*MnSODc was determined to be 1.0×10^9 $M \cdot s^{-1}$ by following the appearance of Mn^{3+}SOD (λ_{max} = 480 nm; see method, Figure S3) as *Ca*Mn^{2+}SODc was oxidized by substoichiometric amounts of O_2^-. However, at physiological pH (6.5–7.5), *Ca*MnSODc removed various concentrations of O_2^- ($[O_2^-]$:[MnSOD] from 2–48:1) at similar rates, showing that only minimal product inhibition occurred under these conditions. Even at $[O_2^-]$:MnSOD ratios as high as 48, the activity of *Ca*MnSODc was comparable to that of *S. cerevisiae* CuZnSOD, an enzyme that does not exhibit product inhibition (Figure S4). The disappearance of O_2^- catalyzed by *Ca*MnSODc could be fitted to a first-order process.

To achieve such a high efficiency, *Ca*MnSODc would either carry such a high gating ratio (k_2/k_3) that the reaction of Mn^{2+}SOD with O_2^- proceeds almost completely via the fast protonation (reaction 2), or it has such a high dissociation rate (k_4) that the product-inhibited complex decomposes before it is detected during pulse radiolysis (reaction 4). Assuming that k_4 is 50 s^{-1}, which is close to that of bacterial dimeric MnSODs, the calculated k_2/k_3 is 65. Assuming that k_2/k_3 is 20, which is comparable to that for *Sc*MnSOD, k_4 is calculated to be 210 s^{-1}. The latter scenario is more likely, because a dissociation rate of 210 s^{-1} is not dramatically different from a k_4 of 130 s^{-1} for human MnSOD and 90-140 s^{-1} for *Sc*MnSOD. In addition, dissociation rates as large as 1000 s^{-1} have been reported in human Y34 mutants.[24] A k_2/k_3 ratio of 65, however, is three times as large as the gating ratio of *Sc*MnSOD, the least inhibited MnSOD that has been characterized to date. Therefore, the high efficiency of *Ca*MnSODc is more likely due to the fast dissociation of the inhibited complex from the metal center.

Previous studies have shown that the rate of enzymatic catalysis as a function of pH is different for the human and bacterial MnSODs. Given that a major difference between the human and bacterial MnSODs is that the former is a tetramer while the latter are dimers, we compare here two yeast MnSODs, where one is a dimer and the other is a tetramer. In these studies we were initially interested only in the change in the fast catalytic cycle (k_1 and k_2), which was measured by following the disappearance of O_2^- in the presence of *Sc*MnSOD or *Ca*MnSODc under conditions where the $[O_2^-]$:MnSOD ratio was between 1 and 3. The overall activity of both *Sc*MnSOD and *Ca*MnSODc decreased considerably as pH was increased (Figure 3). Both yeast enzymes resemble *Ec*MnSOD, with a relatively constant activity up to pH 9, but are distinct from human MnSOD, where catalysis is relatively unchanged even up to pH 11. It is surprising that *Sc*MnSOD and *Ca*MnSODc are different in their quaternary structure, yet they exhibit such similar pH dependence. It is notable that the yeast MnSODs are even more sensitive to the change of pH than the bacterial MnSODs. The p*K* is ~8.5 in two yeast MnSODs, ~9.5 in *Ec*MnSOD and ~10.5 in human MnSOD. Adjusting the pH of yeast MnSOD sample solutions from 9.5 back to 7 resulted in the restoration of their activity to ~50% of that of the intact enzymes (Figure 3).

pH also has an impact on the level of product inhibition exhibited by *Sc*MnSOD. The slow almost zero-order phase, which is a sign of the saturation of MnSOD by O_2^-, was

discernable from the reaction of high concentrations of O_2^- ([O_2^-]:MnSOD = 48:1) with *Sc*MnSOD at pH 8.9 (Figure 4). This feature was barely seen under the same conditions at pH 7.5. The gating ratio k_2/k_3 and the dissociation rate k_4 were calculated by fitting the O_2^- decay into the four-reaction mechanism (Scheme 2; Figure 4, inset). The calculated k_2/k_3 is a constant value over the pH range of 7–9.5. The dissociation rate k_4, however, dramatically decreases when pH is raised to 8 and reaches a plateau at pH ~8.5 with a p*K* of ~8. Due to a depressed k_4, the dissociation of H_2O_2 from the active site may become the rate-limiting step at high pH, resulting in a more inhibited *Sc*MnSOD. The values of k_2/k_3 and k_4 of *Sc*MnSOD were difficult to calculate at pH > 9.5, at which point k_1 and k_2 corresponded to the rate-limiting steps of the reaction. In the case that k_4 stays constant at the plateau while k_1, k_2 and k_3 continue decreasing at pH >9.5, the dissociation of the inhibited complex may occur faster than its formation, leading to a decay of O_2^- at pH >9.5 that appeared to be non-inhibited.

*Ca*MnSODc, in contrast, did not show a pronounced occurrence of the slow zero-order phase even at elevated pH (Figure S5). The decay of O_2^- over the pH range of 7–9.5 could still be fit to a first-order process (R^2 = 1.5). In this case it is difficult to calculate either the ratio of k_2/k_3 or the value of k_4 based on fitting.

Oxidation State

Our previous work showed that tetrameric *Sc*MnSOD, unlike all other wild-type MnSODs studied thus far, is isolated predominantly in the 2+ oxidation state.[4] Dimeric *Ca*MnSODc, structurally similar to bacterial MnSODs, is also isolated in the Mn^{2+} state (Figure S6-A). The two enzymes from yeast are also very similar with respect to the thermodynamics of oxidation and reduction. From this point on, if the results are very similar for the two yeast MnSODs, data from only one enzyme are shown.

The optical absorption spectrum of as-isolated *Sc*MnSOD has a very weak visible absorption band around 480 nm (Figure 5A) that suggests that a small amount of Mn^{3+}SOD is present along with a significantly larger amount of Mn^{2+}SOD. The addition of sodium hyposulfite fully reduced the enzyme and completely quenched this absorption intensity (Figure 5A). Based on the difference in absorption between the fully reduced and the as-isolated enzyme (Figure 5A, insert) and using the extinction coefficient for Mn^{3+}SOD obtained from pulse radiolysis (ε_{475} = 780 $M^{-1}cm^{-1}$), ~5% of the as-isolated enzyme is oxidized. The oxidized enzymes found in both asisolated *Sc*MnSOD and *Ca*MnSODc have spectra that differ from those of most reported Mn^{3+}SODs in that additional absorption intensity at ~390 nm is visible (Figure 5A, inset; Figure S6-A, inset). They are, however, similar to the spectrum of *Sc*Mn^{3+}SOD that was reported previously.[25]

Oxidation of as-isolated *Sc*Mn^{2+}SOD or *Ca*Mn^{2+}SODc by 0.75 equivalents of potassium permanganate rapidly gave absorption spectra characteristic of 5-coordinate Mn^{3+}SOD with a maximum at 480 nm (Figure 5B, S6-B) with no residual absorbance of permanganate. Both yeast MnSODs remained oxidized in solution and retained full activity as determined by pulse radiolysis. Interestingly, an absorption intensity around 390 nm increased slowly over time (Figure 5B, S6-B). Based on the difference between the immediately scanned and the final spectrum (Figure S7), a Mn^{3+}-containing species different from the 5-coordinate Mn^{3+}SOD was formed over time. Further addition of 1 equivalent of sodium ascorbate selectively bleached the absorption of *Sc*Mn^{3+}SOD or *Ca*Mn^{3+}SODc around 390 nm, yielding the characteristic 5-coordinate Mn^{3+}SOD spectrum (Figure 5C, S6-C), which has been reported previously.[25] Treatment of the yeast enzymes with 10-fold molar excess of ascorbate yielded the completely reduced enzymes. Therefore, the unknown species is kinetically more prone to reduction by ascorbate than the well-characterized 5-coordinate species. In contrast, In contrast, 0.5 equivalent of H_2O_2 reduced the 5-coordinate Mn^{3+} and

the unknown species simultaneously in one equivalent of yeast Mn^{3+}SODs, giving optical spectra of full reduced MnSOD (data not shown). The slow formation of the 6-coordinate adduct and its susceptibility to reduction by ascorbate are very puzzling, and we will continue exploring the explanation in future.

One species known to absorb around 390 nm is the low-temperature *Ec*Mn^{3+}SOD:azide adduct. At room temperature, the 5-coordinate *Ec*Mn^{3+}SOD binds azide in such a fashion that the coordination number of the Mn ion does not change. At lower temperatures (p*K* = 200 K) this adduct transforms into an inner-sphere 6-coordinate azide-Mn^{3+}SOD complex.[26] The room-temperature spectrum of azide-treated *Sc*Mn^{3+}SOD shows a shift of the absorption band similar to that observed in other azide-Mn^{3+}SODs[26] (Figure S8). However, there remains additional intensity at 390 nm that is reminiscent of the features present in the spectrum of the low-temperature azide adduct of *Ec*Mn^{3+}SOD where azide is directly bound to the Mn ion. This may indicate that the unknown species in *Sc*Mn^{3+}SOD is also 6-coordinate.

The measurement of the redox potential of MnSOD is notoriously difficult. Our electrochemical studies on *Sc*MnSOD and *Ca*MnSODc failed to achieve efficient electron transfer between the electrode and the enzymes and thus only yielded an approximation of their redox potential as ~0.3 V. This value is comparable to those determined for *E. coli* (0.3 V)[27] and human (0.4 V)[28] MnSOD, which are a reflection of the redox potential of the 5-coordinate Mn^{3+}SOD species. The redox potentials of human and *E. coli* MnSOD are close to that of ascorbate$^{\bullet-}$, H^+/ascorbateH^- ($E°$ = 282 mV) at neutral pH.

The Mn^{3+}SOD spectra obtained from pulse radiolysis, in which *Sc*Mn^{2+}SOD or *Ca*Mn^{2+}SODc was oxidized by substoichiometric amount of O_2^- (see method), merely showed formation of the well characterized 5-coordinate Mn^{3+}SOD[4] and were comparable to those of other Mn^{3+}SODs[3,29] (Figure 6). However, the time scale of each single measurement at each wavelength was shorter than 1 ms. Over 10 ms the reduction of yeast Mn^{3+}SODs by excess H_2O_2 was discernable. Therefore, the generation of the putative L-Mn^{3+}SOD species likely occurred more slowly under pulse radiolysis conditions than the reduction of the 5-coordinate Mn^{3+} center by H_2O_2. Indeed the shifting of the spectrum around 390 nm was discernable in a much longer timescale (> 10 min) from the oxidation of asisolated *Sc*MnSOD using ^{60}Co radiation as the source of O_2^- (Figure S9).

MnSODs that are isolated in the Mn^{3+} state possess absorption spectra that change modestly as pH is raised. For example, at pH > 9 the 478 nm absorption feature corresponding to *Ec*Mn^{3+}SOD begins to diminish slightly in intensity and shifts to shorter wavelength. This p*K* event has been ascribed to deprotonation of Tyr34 (numbering in *Sc*MnSOD).[30] However, for *Sc*MnSOD and *Ca*MnSODc the absorption intensity around 390 nm increased as pH was increased (Figure 5D, S6-D). *Sc*MnSOD and *Ca*MnSODc may not have the same p*K* as other Mn^{3+}SODs, or the spectral change due to the p*K* may have been obscured by the absorption shifting around 390 nm. The Mn^{3+} spectra of *Sc*MnSOD obtained from pulse radiolysis at pH 7 and 10 were compared, and a roughly 20% decrease in intensity but no shift in peak for the Mn^{3+}SOD absorbance at 480 nm were observed (Figure S10). The spectral shift over pH indicates that the sixth ligand is likely a hydroxide that with a higher concentration binds to Mn^{3+} more readily at high pH.

EPR Spectra

In agreement with the electronic absorption data shown above, results from perpendicular-mode X-band EPR experiments confirm that *Ca*MnSODc is isolated pre-dominately in the Mn^{2+} oxidation state (Figure S11-A). These spectra are similar to those obtained for *Ec*Mn^{2+}SOD with five separate electronic spin transitions observed due to zero- field

splitting of the manifold of spin levels of the high-spin (S = 5/2) Mn^{2+} ion. These resonances are further split by the hyperfine interaction of the electron spin with the ^{55}Mn nuclear spin (I = 5/2). The corresponding parallel-mode EPR spectrum for as-isolated *Ca*MnSODc possesses little intensity (Figure S11-B). In contrast, the spectra of the pH 7.65 permanganate-oxidized samples have at least eight intense transitions centered at 80 mT (g = 8.4) (Figure 7A) that are somewhat similar to the six parallel-mode EPR transitions separated by ≈10 mT observed previously for *Ec*Mn^{3+}SOD.[31] Campbell *et al*,[31] showed that these signals arise from transitions within the $m_S = |\pm 2\rangle$ manifolds of a high-spin (S = 2) Mn(III) system. Analysis of the temperature-dependence of the integrated signal intensity led to an evaluation of the magnitude and, importantly, sign of the zero-field splitting parameters—D = +2.10 cm^{-1} and E = 0.24 cm^{-1}. (NOTE: These values are consistent with those determined by analysis of variable-temperature, variable-field magnetic circular dichroism saturation behavior.[32]) That $D > 0$ indicates that the lowest unoccupied metal-centered molecular orbital (MO) is $3d_z^2$-based.[33] These conclusions are borne out by the trigonal bipyramidal coordination geometry of the Mn^{3+} site determined by X-ray crystallography as well as results of numerous electronic structure calculations.[34]

In the present case of *Sc*Mn^{3+}SOD and *Ca*Mn^{3+}SODc, more than six parallel-mode resonances are observed, indicating that there are at least two Mn^{3+}-containing species present in the sample. Subtraction of the EPR spectrum of *Ec*Mn^{3+}SOD from that of *Sc*Mn^{3+}SOD reveals an underlying sextet with interpeak spacings of approximately 4.5–5.0 mT (Figure 7B). Such a small effective ^{55}Mn hyperfine coupling parameter ($A_\parallel$) has been observed previously for several 6-coordinate Mn(III) centers.[33,35,36] There has also been a preliminary report that showed a fraction of 5-coordinate *Ec*Mn^{3+}SOD converts to a new species at pH 11.54 that is characterized by a parallel-mode EPR spectrum with $A_\parallel$ (^{55}Mn) = 3.3 mT.[31]

The dramatic difference in $A_\parallel$ for the two spectroscopically distinct *Sc*Mn^{3+}SOD species is likely resulted from a change in the electronic ground state for the Mn^{3+} ion—from $5A_{1g}$ to $5B_{1g}$.[33] Respectively, these states correspond to d-electron configurations wherein the $3d_z^2$-based and $3d_x^2 - y^2$-based MOs are empty. A simple explanation for this change would be a new, strong ligand binding in the equatorial plane to the Mn^{3+} ion. This event would raise the energy of the $3d_x^2 - y^2$-based MO allowing the fourth d-electron to occupy the $3d_z^2$ orbital instead.

The EPR transition observed for both electron configurations is between the $m_S = |\pm 2\rangle$ spin levels. For the $5B_{1g}$ state, the axial zero-field splitting interaction (D) will be negatively signed, putting the $|\pm 2\rangle$ manifold lowest in energy. Thus this manifold will be populated at all temperatures and if the energy splitting (Δ) of the $m_S = |\pm 2\rangle$ spin levels at zero field is less than the energy of the incident microwave radiation ($h\nu$ = 0.319 cm–1 for the 9.396 GHz radiation employed here) a parallel-mode EPR transition will be observed. However, for the $5A_{1g}$ state, the sign of D is positive and the $|\pm 2\rangle$ manifold will not be populated at low temperatures. For *Ca*Mn^{3+}SODc, increasing the temperature thermally populates this manifold and the EPR transition becomes apparent. By monitoring the temperature-dependent intensity of the peak at 58 mT we have determined that D = +1.90 cm^{-1} and E = 0.20 cm^{-1}, values similar to those found for the 5-coordinate form of *Ec*Mn^{3+}SOD (see Figure S12).

Upon treatment of *Sc*Mn^{3+}SOD with 1 equivalent of ascorbate, the $5B_{1g}$ contribution to the parallel-mode EPR spectrum completely disappears (compare second and third traces in Figure 7A). This spectral change coincides with bleaching of the 390 nm feature in the electronic absorption spectrum (Figure 5C) upon addition of ascorbate, suggesting the

narrowly split EPR signal and the 390 nm absorption intensity are spectral signatures of the same species.

Crystal Structure

The active site structure of the two yeast MnSODs was investigated by crystallography (Table S1). The crystals of both yeast MnSODs are colorless. The X-ray crystallography structure of *Sc*MnSOD is always a tetramer (Figure S13-A). To our surprise, the quaternary structure of *Ca*MnSODc varied with crystallization conditions. It is either a dimer (data not shown) or a tetramer (Figure S13-B). We believe that the quaternary structure of *Ca*MnSODc depends on buffer condition (ion strength and viscosity) and protein concentration, and we will explore the factors that control its quaternary structure in a future publication.

*Sc*MnSOD and *Ca*MnSODc both maintain the 5-coordinate sphere of manganese conserved in all other MnSODs (Figure 8).[34,37-40] Their active sites are superimposable, giving a root mean square deviation (RMSD) of 0.20 Å (Figure S14). For both enzymes the observed manganese bond lengths are ~2.2 Å to each His NE2, 2.0 Å to Asp OD2, and 2.3 Å to OH2 (Table S2). These are only slightly longer than the corresponding distances in MnSODs that rest predominantly in the Mn^{3+} state. Spectroscopic and computational evidence suggests that in the reduced state Mn is bound by a water molecule and in the oxidized state it is bound by a hydroxide.[41] The distance of the Mn–O bond should be farther in the bound water as it is not as strong a bond and closer in the bound hydroxide. The long Mn–O (solvent molecule) distances in both yeast MnSODs are consistent with Mn^{2+}–OH_2 moieties. Although these shifts are small and within possible experimental error, the observed longer coordination bond distances could reflect the 2+ oxidation state of *Sc*MnSOD and *Ca*MnSODc.

During X-ray crystallography data collections, metalloenzyme crystals are likely to be reduced by photoelectrons generated from the excitation of protein and solvent atoms by the incident X-ray beam.[42] As *Sc*MnSOD and *Ca*MnSODc are both isolated in the reduced form as indicated by their optical and EPR spectra (Figure 5, S6 and S11), the X-ray structures are certainly those of the reduced (Mn^{2+}SOD) enzymes. For other MnSODs that are isolated in the Mn^{3+} oxidation state, active site bond distances measured in their X-ray structures (Table S2) would suggest that the human and *Thermus thermophilus* crystals contained primarily Mn^{3+}SOD and the remaining MnSODs were likely primarily reduced during the data collection.

DISCUSSION

The Relationship of Product Inhibition to Active Site Structure

Based on the structural and sequence similarity shared between *Sc*MnSOD and human MnSOD, *Sc*MnSOD was expected to exhibit a level of product inhibition similar to human MnSOD. However, we found that *Sc*MnSOD is dramatically gated toward the fast protonation pathway. *Ca*MnSODc resembles *Sc*MnSOD in its efficiency of removing O_2^- at high O_2^- doses. The yeast MnSODs are more like bacterial MnSODs in terms of function. Our studies on yeast MnSODs place human MnSOD in a unique class that predominantly undergoes the product-inhibited pathway at high levels of O_2^- among MnSODs that have been characterized to date.

Numerous studies on the structure-function relationship of MnSOD have been focused on the structure of second coordination sphere structure,[24,43-47] which is highly conserved in MnSOD from different organisms.[34,37-39] Superposition of all active site residues (within 6 Å of Mn) of *Sc*MnSOD on those of human or *E. coli* MnSOD gives RMSD of 0.25 and 0.18

Å, respectively (Figure 9), indicating that in terms of second coordination sphere, *Sc*MnSOD resembles *Ec*MnSOD more than it does human MnSOD, in spite of the fact that *Sc*MnSOD and human MnSOD are both tetramers and share greater sequence similarity. Of particular significance are highly conserved residues Tyr34 and His30, mutations of which usually cause changes in product inhibition.[24,48] Their positions in *Sc*MnSOD overlap more with those in *Ec*MnSOD than with those in human MnSOD (Figure 9). One would expect subtle shifts of these residues in the second coordination sphere to cause dramatic differences in the degree of product inhibition among MnSOD from different species. The factors that control the level of product inhibition will be subjects of future investigations.

The Unusual Resting State of Yeast MnSODs and the Role of Gln154

In contrast to human and bacterial MnSODs that rest predominantly as Mn^{3+}SOD, the as-isolated proteins of yeast MnSODs are both ~95% reduced. Our preliminary electrochemical results indicate that the redox potentials of yeast MnSODs are comparable to those determined for human and bacterial MnSODs. However, previous studies on *Ec*MnSOD have shown spontaneous oxidation of *Ec*Mn^{2+}SOD in air[29], which does not occur in yeast MnSODs. Therefore, the unusual resting state of the yeast enzymes may result from thermodynamically driven shifts in oxidation-reduction equilibria.

The fact that yeast MnSODs rest as Mn^{2+}SOD could be linked with the positioning of an outer-sphere residue, Gln154 (the numbering in *Sc*MnSOD; *Ca*MnSODc: Gln163; human: Gln143; *E. coli*: Gln146). Conserved in all Mn and FeSODs, Gln154 donates an H-bond to the metal-bound solvent molecule, and is the only contact of the metal-bound solvent molecule to the protein beyond the active site. Gln154 makes three hydrogen bonds to three highly conserved residues, Tyr34, Asn80 and Trp133 (numbering in *Sc*MnSOD). Its hydrogen bonding potential is fully utilized and Gln154 seems firmly fixed in place. Gln154 together with Asp168 that is an H-bond acceptor from the metal-coordinated H_2O or OH^-, determine the position of the coordinated solvent molecule. Mutagenesis on Gln154 often causes dramatic depression of reactivity,[43,44,46] indicating the key role of the NE2(Gln154)···O(solv) bond.

The active site reduction midpoint potential (E_m) contributes directly to the driving forces of the two half reactions of O_2^- dismutation. In Mn and FeSOD (structural homologs), Gln154 is critical in modulating E_m and thus contributes to the ion specificity as well as determining the resting state of Mn and FeSOD.[12,49] The second coordination sphere of Mn and FeSOD is similar except that the Gln154 amide nitrogen is ~0.7 Å further from the metal in FeSOD. DFT calculations on the structure of Mn and FeSOD suggest the reason of MnSOD resting predominantly in the Mn^{3+} state as the destabilization of coordinated H_2O vs. OH^- by the closely placed glutamine side chain.[12,50] In Mn-substituted *Ec*FeSOD in which Mn is placed away from Gln69, the E_m is elevated by 670 mV and the enzyme completely rests as the reduced form.[51] Mutation of Gln143 to asparagine in human MnSOD also causes the enzyme to rest as Mn^{2+}SOD.[43] Either *Ec*Mn(Fe)SOD or human Q143 mutants is only able to catalyze one half reaction, the oxidation of O_2^-.[43,51]

Most MnSODs with solved structure conserve a NE2(Gln154)···O(solv) H-bond of 2.85–2.95 Å (Table S2), and, as indicated by previous studies, the further the Gln154 amide nitrogen is away from Mn, the more the 2+ state is favored by the enzyme. Thus, the observation that the distance of Gln154 to Mn is slightly longer in the two yeast MnSODs (4.79 and 4.73 Å in *Sc*MnSOD and *Ca*MnSODc, respectively) than in the MnSODs that predominantly rest in the oxidized form (Human: 4.65 Å; *E. coli*: 4.64 Å; *D. radiodurans*: 4.54 Å; *Caenorhabditis elegans*: 4.54 Å) may be related to fact that the yeast MnSODs rest in the reduced state.

The Relationship of Product Inhibition of Human MnSOD to H_2O_2 Signaling in Mammals

Human MnSOD is much less efficient at turning O_2^- into H_2O_2 than *Sc*MnSOD when O_2^- levels are high, although the two enzymes share great sequence similarity and are both located in mitochondria. Mitochondria are recognized as the source of O_2^- with the production occurring through respiratory chain. H_2O_2 is generated in mitochondrial matrix via the dismutation reaction of O_2^- catalyzed by MnSOD. The produced H_2O_2 then diffused into cytosol. The roles of H_2O_2 are complex in higher organisms. In mammalian cells the upregulated expression of antioxidant enzymes is not a universal response to supraphysiologic levels of H_2O_2.[7] Instead, physiologic levels of H_2O_2 stimulate cell division, transformation, migration or apoptosis.[7,8,10,11] This along with the fact that mammalian cells generate H_2O_2 in response to various stimuli supports that H_2O_2 is utilized as a signaling agent in numerous mammalian signaling pathways.[7-11,52,53] A well established H_2O_2-induced signaling is the modulation of the tyrosine phosphorylation of proteins by causing the oxidative inhibition of tyrosine phosphatases.[9] Reversible inactivation of tyrosine phosphatases has been demonstrated to play a critical role in PTP and insulin signaling.[54,55] Several mitochondrial signaling pathways are stimulated by increased H_2O_2, including tumor necrosis factor (TNF)-α-induced apoptosis[56] and c-Jun NH_2-terminal kinase (JNK)-induced apoptosis.[52,57] The participation of H_2O_2 in signaling cascades may require tight regulation of its production in mitochondria.

A recent study demonstrates the production of large bursts of O_2^-, termed “superoxide flashes”, in human mitochondria.[58] The events of superoxide flashes occur randomly in space and time, last for 20–30 seconds and are confined to tiny elliptical areas.[58] Under the conditions that were tested human MnSOD in mitochondrial matrix was expected to eliminate superoxide flashes in a shorter time scale, considering that the reactivity of human MnSOD was thought to be diffusion controlled ($k = 2.3 \times 10^9\ M^{-1}\ s^{-1}$) and its intramitochondrial concentration is 10–40 μM.[52,59] The observation of superoxide flashes indicates that human MnSOD is unable to maintain a steady-state concentration of O_2^- in tiny elliptical areas in mitochondria. The most likely explanation for this phenomenon is that human MnSOD is significantly inhibited at these high concentrations of O_2^-. Under these conditions, bursts of O_2^- are not translated into bursts of H_2O_2 that could result in aberrant oxidant-driven signaling in mitochondria.

Mitochondria are the main source of H_2O_2 and its decomposition in the mitochondrial matrix is catalyzed by glutathione peroxidase and catalase. The rate constants of mammalian glutathione peroxidase and catalase are $5 \times 10^7\ M^{-1}\ s^{-1}$ and $4.6 \times 10^7\ M^{-1}\ s^{-1}$, respectively, and their intramitochondrial concentration is ~10% that of MnSOD.[59] These antioxidants maintain a steady-state intramitochonrial H_2O_2 concentration of $\sim 0.5 \times 10^{-8}$ M.[59] As no comparison of H_2O_2 concentration in areas with or without superoxide flashes has been reported, it is unclear whether superoxide flashes cause “H_2O_2 flashes ” in tiny confined areas in mitochondria.

In contrast, neither superoxide flashes nor evidence of H_2O_2 signaling in yeast have been reported. The different levels of product inhibition found in human and *Sc*MnSOD may well be explained by the necessity for constrained generation of H_2O_2 in human mitochondria, especially under the conditions associated with “superoxide flashes”.

Binding of a Sixth Ligand and the Proposed Mechanism of Yeast MnSODs

Native *Sc*Mn^{3+}SOD and *Ca*Mn^{3+}SODc display optical absorption spectra that are different from other Mn^{3+}SODs. When the yeast enzymes were chemically oxidized, the spectra changed over time from characteristic 5-coordinate Mn^{3+} spectra to spectra with additional absorption intensity around 390 nm. The growth of this absorption intensity can be ascribed

to the binding of a sixth ligand, L, leading to formation of an L-Mn^{3+}SOD complex, and since its formation is favored at high pH the sixth ligand is highly likely to be a hydroxide. EPR spectra suggest the presence of at least two Mn^{3+}-containing species with distinct electronic ground states in yeast Mn^{3+}SODs. One of them is the well-characterized 5-coordinate Mn^{3+}SOD, and the other could be an L-Mn^{3+}SOD species with the sixth ligand bound in the equatorial plane.

A 6-coordinate MnSOD that binds two H_2O/OH^- has been obtained in the past at cryogenic conditions or at high pH. The structure of cyro-trapped *Ec*MnSOD crystallized at pH 8.5 shows a H_2O/OH^- bound to the equatorial plane of Mn, giving an octahedral coordination center.[60] Probing the Mn^{2+} center of *Ec*MnSOD using high-field EPR indicates transfer of a water molecule to the Mn center at 240–268 K.[61] *Ec*Mn^{3+}SOD at pH 11.65 forms a putative 6-coordinate species, giving a heterogeneous EPR spectrum that is comparable to those reported here for *Sc*Mn^{3+}SOD and *Ca*Mn^{3+}SODc at pH 7.65.[31] Recently Porta *et. al.* have reported a 6-coordinate structure of *Ec*MnSOD with peroxide bound as a side-on ligand to active site manganese.[62] However, the existence of a 6-coordinate MnSOD binding two H_2O/OH^- that is stable in solution at room temperature and neutral pH is novel.

Examination of the second coordination sphere of *Sc*MnSOD shows two outer-sphere solvent molecules within 6 Å of the Mn center, in addition to the Mn-coordinated water. As discussed by Tabares *et. al.*,[61] the sixth ligand is most likely the water that is hydrogen bonded to Tyr34 and His30 (Figure 8). Tyr34 and His30 are highly conserved residues that are part of the proposed hydrogen-bonding network, which pumps protons from protein surface to active site.[1,40,45,46] They are also involved in the gating between fast and slow protonation pathways as well as the dissociation of H_2O_2 from the active site.[24,48] This water, however, only occupies 50% of the subunits in the structure of *Sc*MnSOD or *Ec*MnSOD and cannot be seen in the structure of human MnSOD or *Ca*MnSODc.

The binding site of O_2^- in the MnSOD active site has been investigated using small anions like fluoride and azide as O_2^- analogues. Azide binds to the sixth ligand site in proximity of Try34 in the plane of His26, His81 and Asp168 at low temperatures.[26] Fluoride also sits close to the same binding site and is likely hydrogen bonded to Tyr34.[63] Therefore, to react with the Mn ion O_2^- is highly likely bound in the sixth ligand site in the vicinity to Tyr34. O_2^- has also been proposed to form hydrogen bonds with Tyr34 and the Mn-coordinated H_2O but does not directly bind Mn.[63] In both cases, the outer-sphere water, which has been proposed to become the sixth ligand, is located in the vicinity to the O_2^- binding site.

Herein we propose a mechanism based on the tendency of yeast Mn^{3+}SODs to bind two solvent molecules, which may explain their high efficiency at high O_2^- doses (Scheme 3). When O_2^- binds to (or merely approaches) the sixth ligand binding site close to Tyr34, Mn^{2+} transfers an electron to O_2^- (which becomes peroxide) and is oxidized to Mn^{3+}. Since Mn^{3+}SOD tends to bind two solvent molecules, the water molecule that is hydrogen bonded to Tyr34 and His30 may travel to the Mn^{3+} center to compete with the peroxide for the sixth ligand site (Scheme 3). This could cause steric effects at the metal binding site, which may destabilize the inner-sphere peroxo-Mn^{3+}SOD complex. This is consistent with the fact that *Sc*MnSOD and *Ca*MnSODc are significantly gated toward the outer-sphere fast protonation pathway, in which formation of the peroxo-Mn^{3+}SOD species is disfavored. The outer-sphere water may not necessarily bind Mn^{3+} ion, which could be a slow process, but merely fluctuate between the Mn center and Tyr34/His30 to create steric effects at the active site. Deviations in the positioning of outer-sphere solvent molecules have been reported to be important in enhancing proton transfer in other metalloenzymes.[64] In human carbonic anhydrase II (HACII), the positioning and structuring of water molecules in the active site cavity vary with the conformation of an outer-sphere residue, His64.[64]

The putative translocation of the outer-sphere solvent molecule in yeast MnSODs may also facilitate dissociation of the bound peroxide by enhancing proton transfer. Numerous previous studies show that MnSODs from various organisms exhibit a similar hydrogen isotope effect of ~2, suggesting that proton transfer is involved.[65] Dissociation of H_2O_2 from MnSOD active site requires two protons transferred from the protein. Rapid proton transfer from the axial solvent ligand to peroxide is expected to occur in all MnSOD. In yeast MnSODs the other proton is likely donated by the outer-sphere H_2O that sits between Tyr34 and His30 upon translocation, which may highly enhance the proton transfer and facilitate the removal of the peroxide from the active site.

Indeed, the rate of peroxide release from active site (k_4) in *Sc*MnSOD is dramatically depressed at increased pH with a p*K* of ~8, which causes the level of product inhibition to increase (Figure 4). This is significantly different from human MnSOD, which maintain a constant k_4 over a wide range of pH (6–10).[65] The depression of k_4, which is likely caused by slower proton transfer, could either be resulted from deprotonation of the axial H_2O or the outer-sphere H_2O that is hydrogen bonded to Tyr34 and His30, or from deprotonation of Tyr34 as proposed to be responsible for the spectroscopic p*K* of *Ec*MnSOD.[30303030] In the latter scenario, deprotonation of Tyr34 may destabilize the potential sixth ligand by eliminating its hydrogen bonding with Tyr34. Considering that the p*K* of k_4 for *Sc*MnSOD is as low as 8 (Figure 4) while the p*K* of Tyr34 is 11.5, deprotonation of the solvent ligands is more likely. This may support the hypothesis that the outer-sphere solvent molecule approaches the sixth ligand site of the Mn^{3+} ion and transfers a proton to the peroxide to facilitate its leaving.

However, the binding of two H_2O/OH^- in *Sc*Mn^{3+}SOD and *Ca*Mn^{3+}SODc may not be relevant to their fast catalytic kinetics and low level of product inhibition, but merely a coincidence. We will therefore continue investigating the correlation between product inhibition and the L-Mn^{3+}SOD species by investigating yeast MnSOD mutants with mutations at certain second coordination sphere residues.

In conclusion, MnSODs from *S. cerevisiae* mitochondria and *C. albicans* cytosol both exhibit higher efficiencies of O_2^- dismutation at high [O_2^-] than human and bacterial MnSODs. The unusual resting state of yeast MnSODs could be attributed to the slightly longer distance between Gln154 and Mn. Both yeast Mn^{3+}SODs form a 6-coordinate species. The potential sixth ligand could be an outer-sphere water and its translocation to Mn ion in the catalytic cycle may facilitate the reaction of Mn^{2+}SOD with O_2^- to undergo through the non-inhibited pathway. Among MnSODs that have been characterized to date, human MnSOD is the only enzyme that significantly undergoes the product-inhibited pathway at high [O_2^-], which can be ascribed to complicated roles of H_2O_2 in mammalian cells, especially as a signaling agent.

Supplementary Material

Refer to Web version on PubMed Central for supplementary material.

Acknowledgments

This work was supported by Grant DK46828, KOSEF/MEST through WCU project (R31-2008-000-10010-0) to J.S.V. and National Institutes of Health and Grant GM48242 to R.D.B. Radiolysis studies were carried out at the Center for Radiation Chemistry Research at BNL, which is funded under Contract DE-AC02-98CH10886 with the U.S. Department of Energy and supported by its Division of Chemical Sciences, Geosciences, and Biosciences, Office of Basic Energy Sciences. We acknowledge Minglei Zhao (Department of Chemistry and Biochemistry, UCLA) in assisting us in the X-ray structural determination. We acknowledge Professor Michael Hill (Occidental College) in assisting us in the redox potential measurements.

References

(1). Abreu IA, Cabelli DE. Biochim Biophys Acta. 2010; 1804:263. [PubMed: 19914406]

(2). Zheng J, Domsic JF, Cabelli D, McKenna R, Silverman DN. Biochemistry. 2007; 46:14830. [PubMed: 18044968]

(3). Abreu IA, Hearn A, An H, Nick HS, Silverman DN, Cabelli DE. Biochemistry. 2008; 47:2350. [PubMed: 18247479]

(4). Barnese K, Sheng Y, Stich TA, Gralla EB, Britt RD, Cabelli DE, Valentine JS. J Am Chem Soc. 2010; 132:12525. [PubMed: 20726524]

(5). Valko M, Rhodes CJ, Moncol J, Izakovic M, Mazur M. Chem Biol Interact. 2006; 160:1. [PubMed: 16430879]

(6). Giorgio M, Trinei M, Migliaccio E, Pelicci PG. Nat Rev Mol Cell Biol. 2007; 8:722. [PubMed: 17700625]

(7). Veal EA, Day AM, Morgan BA. Mol Cell. 2007; 26:1. [PubMed: 17434122]

(8). Stone JR, Yang S. Antioxid Redox Signal. 2006; 8:243. [PubMed: 16677071]

(9). Rhee SG. Science. 2006; 312:1882. [PubMed: 16809515]

(10). Finkel T, Holbrook NJ. Nature. 2000; 408:239. [PubMed: 11089981]

(11). Finkel T. Curr Opin Cell Biol. 2003; 15:247. [PubMed: 12648682]

(12). Jackson TA, Brunold TC. Acc Chem Res. 2004; 37:461. [PubMed: 15260508]

(13). Lamarre C, LeMay JD, Deslauriers N, Bourbonnais Y. J Biol Chem. 2001; 276:43784. [PubMed: 11562375]

(14). Schwarz, H. BNL Pulse Radiolysis Program. Brookhaven National Laboratory;

(15). Stoll S, Britt RD. Phys Chem Chem Phys. 2009; 11:6614. [PubMed: 19639136]

(16). Stoll S, Schweiger A. J Magn Reson. 2006; 178:42. [PubMed: 16188474]

(17). Walter TS, Meier C, Assenberg R, Au KF, Ren JS, Verma A, Nettleship JE, Owens RJ, Stuart DI, Grimes JM. Structure. 2006; 14:1617. [PubMed: 17098187]

(18). Sutherland MW, Learmonth BA. Free Radic Res. 1997; 27:283. [PubMed: 9350432]

(19). Otwinowski Z, Minor W. Method Enzymol. 1997; 276:307.

(20). Mccoy AJ, Grosse-Kunstleve RW, Adams PD, Winn MD, Storoni LC, Read RJ. J Appl Crystallogr. 2007; 40:658. [PubMed: 19461840]

(21). Emsley P, Cowtan K. Acta Crystallogr D. 2004; 60:2126. [PubMed: 15572765]

(22). Murshudov GN, Vagin AA, Dodson EJ. Acta Crystallogr D. 1997; 53:240. [PubMed: 15299926]

(23). Adams PD, Grosse-Kunstleve RW, Hung LW, Ioerger TR, McCoy AJ, Moriarty NW, Read RJ, Sacchettini JC, Sauter NK, Terwilliger TC. Acta Crystallogr D Biol Crystallogr. 2002; 58:1948. [PubMed: 12393927]

(24). Perry JJ, Hearn AS, Cabelli DE, Nick HS, Tainer JA, Silverman DN. Biochemistry. 2009; 48:3417. [PubMed: 19265433]

(25). Ravindranath SD, Fridovich I. J Biol Chem. 1975; 250:6107. [PubMed: 238997]

(26). Whittaker MM, Whittaker JW. Biochemistry. 1996; 35:6762. [PubMed: 8639627]

(27). Vance CK, Miller AF. Biochemistry. 2001; 40:13079. [PubMed: 11669646]

(28). Leveque VJ, Vance CK, Nick HS, Silverman DN. Biochemistry. 2001; 40:10586. [PubMed: 11524001]

(29). Whittaker JW, Whittaker MM. J Am Chem Soc. 1991; 113:5528.

(30). Maliekal J, Karapetian A, Vance C, Yikilmaz E, Wu Q, Jackson T, Brunold TC, Spiro TG, Miller AF. J Am Chem Soc. 2002; 124:15064. [PubMed: 12475351]

(31). Campbell, KA. Dissertation Thesis. University of California-Davis; 1999.

(32). Jackson TA, Karapetian A, Miller AF, Brunold TC. Biochemistry. 2005; 44:1504. [PubMed: 15683235]

(33). Campbell KA, Force DA, Nixon PJ, Dole F, Diner BA, Britt RD. J Am Chem Soc. 2000; 122:3754.

(34). Edwards RA, Baker HM, Whittaker MM, Whittaker JW, Jameson GB, Baker EN. J Biol Inorg Chem. 1998; 3:161.

(35). Krivokapic I, Noble C, Klitgaard S, Tregenna-Piggott P, Weihe H, Barra AL. Angew Chem Int Ed Engl. 2005; 44:3613. [PubMed: 15864797]

(36). Campbell KA, Lashley MR, Wyatt JK, Nantz MH, Britt RD. J Am Chem Soc. 2001; 123:5710. [PubMed: 11403603]

(37). Borgstahl GE, Parge HE, Hickey MJ, Beyer WF Jr. Hallewell RA, Tainer JA. Cell. 1992; 71:107. [PubMed: 1394426]

(38). Fluckiger S, Mittl PR, Scapozza L, Fijten H, Folkers G, Grutter MG, Blaser K, Crameri R. J Immunol. 2002; 168:1267. [PubMed: 11801664]

(39). Trinh CH, Hunter T, Stewart EE, Phillips SE, Hunter GJ. Acta Crystallogr Sect F Struct Biol Cryst Commun. 2008; 64:1110.

(40). Perry JJ, Shin DS, Getzoff ED, Tainer JA. Biochim Biophys Acta. 2010; 1804:245. [PubMed: 19914407]

(41). Jackson TA, Xie J, Yikilmaz E, Miller AF, Brunold TC. J Am Chem Soc. 2002; 124:10833. [PubMed: 12207539]

(42). Carugo O, Djinovic Carugo K. Trends Biochem Sci. 2005; 30:213. [PubMed: 15817398]

(43). Hsieh YS, Guan Y, Tu CK, Bratt PJ, Angerhofer A, Lepock JR, Hickey MJ, Tainer JA, Nick HS, Silverman DN. Biochemistry. 1998; 37:4731. [PubMed: 9537988]

(44). Leveque VJ, Stroupe ME, Lepock JR, Cabelli DE, Tainer JA, Nick HS, Silverman DN. Biochemistry. 2000; 39:7131. [PubMed: 10852710]

(45). Whittaker MM, Whittaker JW. Biochemistry. 1997; 36:8923. [PubMed: 9220980]

(46). Edwards RA, Whittaker MM, Whittaker JW, Baker EN, Jameson GB. Biochemistry. 2001; 40:15. [PubMed: 11141052]

(47). Guan Y, Hickey MJ, Borgstahl GE, Hallewell RA, Lepock JR, O'Connor D, Hsieh Y, Nick HS, Silverman DN, Tainer JA. Biochemistry. 1998; 37:4722. [PubMed: 9537987]

(48). Davis CA, Hearn AS, Fletcher B, Bickford J, Garcia JE, Leveque V, Melendez JA, Silverman DN, Zucali J, Agarwal A, Nick HS. J Biol Chem. 2004; 279:12769. [PubMed: 14688256]

(49). Yikilmaz E, Porta J, Grove LE, Vahedi-Faridi A, Bronshteyn Y, Brunold TC, Borgstahl GEO, Miller AF. J Am Chem Soc. 2007; 129:9927. [PubMed: 17628062]

(50). Yikilmaz E, Xie J, Brunold TC, Miller AF. J Am Chem Soc. 2002; 124:3482. [PubMed: 11929218]

(51). Miller AF, Vance CK. Biochemistry. 2001; 40:13079. [PubMed: 11669646]

(52). Cadenas E. Mol Aspects Med. 2004; 25:17. [PubMed: 15051313]

(53). Droge W. Physiol Rev. 2002; 82:47. [PubMed: 11773609]

(54). Mahadev K, Wu X, Zilbering A, Zhu L, Lawrence JT, Goldstein BJ. J Biol Chem. 2001; 276:48662. [PubMed: 11598110]

(55). Tonks NK. Cell. 2005; 121:667. [PubMed: 15935753]

(56). Melendez JA, Dasgupta J, Subbaram S, Connor KM, Rodriguez AM, Tirosh O, Beckman JS, JourD'Heuil D. Antioxid Redox Sign. 2006; 8:1295.

(57). Chen K, Thomas SR, Albano A, Murphy MP, Keaney JF Jr. J Biol Chem. 2004; 279:35079. [PubMed: 15180991]

(58). Wang W, et al. Cell. 2008; 134:279. [PubMed: 18662543]

(59). Cadenas E, Davies KJ. Free Radic Biol Med. 2000; 29:222. [PubMed: 11035250]

(60). Borgstahl GEO, Pokross M, Chehab R, Sekher A, Snell EH. Journal of Molecular Biology. 2000; 296:951. [PubMed: 10686094]

(61). Tabares LC, Cortez N, Agalidis I, Un S. J Am Chem Soc. 2005; 127:6039. [PubMed: 15839704]

(62). Porta J, Vahedi-Faridi A, Borgstahl GE. J Mol Biol. 2010; 399:377. [PubMed: 20417642]

(63). Tabares LC, Cortez N, Hiraoka BY, Yamakura F, Un S. Biochemistry. 2006; 45:1919. [PubMed: 16460038]

(64). Merz KM, Toba S, Colombo G. J Am Chem Soc. 1999; 121:2290.

(65). Hearn AS, Stroupe ME, Cabelli DE, Lepock JR, Tainer JA, Nick HS, Silverman DN. Biochemistry. 2001; 40:12051. [PubMed: 11580280]

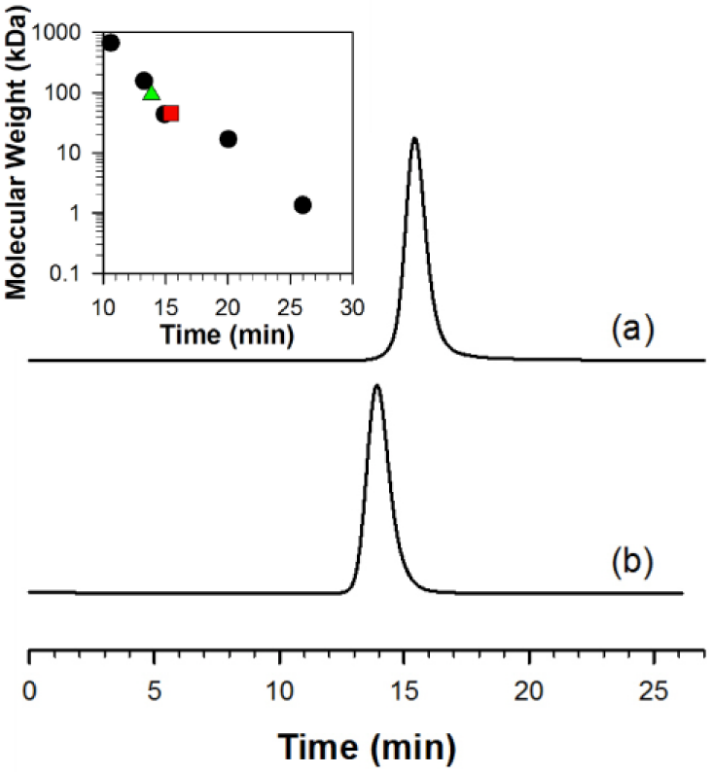

FIGURE 1.

The HPLC-SEC profiles of *Ca*MnSODc (a) and *Sc*MnSOD (b). Inset: The plot of the molecular weight of the five standards (black, circles), *Sc*MnSOD (green, triangle) and *Ca*MnSODc (red, square) versus their retention time. The concentration of proteins loaded into the column is 6 mg/mL. The column was calibrated using five standards: 1) bovine thyroglobulin (670 kDa), 2) bovine γ-globulin (158 kDa), 3) ovalbumin (44 kDa), 4) horse myoglobin (17 kDa), and 5) vitamin B12 (1.35 kDa). The buffer contained 50 mM sodium phosphate (pH 6.7) and 50 mM sodium chloride.

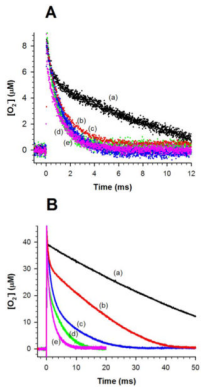

FIGURE 2.

Decay of 7 μM (A) and 41 μM (B) O_2^- catalyzed by 1 μM (in Mn) human (a, black), *E. coli* (b, red), *D. radiodurans* (c, blue) MnSOD, *Sc*MnSOD (d, green) and *Ca*MnSODc (e, pink). The sample for pulse radiolysis contained 10 mM potassium phosphate (pH 7), 10 mM sodium formate and 10 μM EDTA. The O_2^- concentration in these figures is calculated from the absorbance at 260 nm.

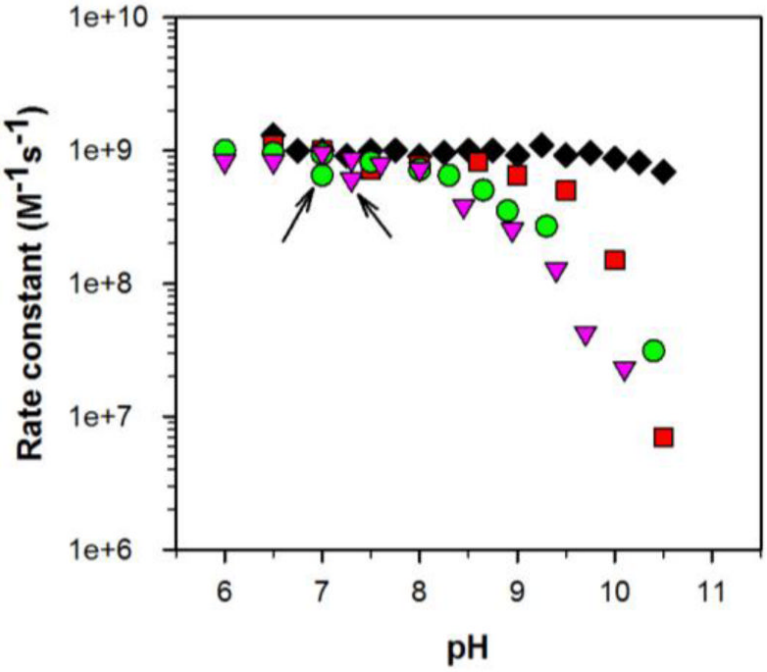

FIGURE 3.

The effects of pH on the overall activity of MnSODs. The rate constant was determined by fitting the disproportionation of low doses of O_2^- ([O_2^-]:MnSOD from 1–3) to a first-order process. Under these [O_2^-]:MnSOD ratios, the reaction of Mn^{2+}SOD with O_2^- proceeds predominantly through the outer-sphere pathway. This rate constant reflects a combination of k_1 and k_2. MnSOD is from human (black, diamonds), *E. coli* (red, rectangles), *S. cerevisiae* (green, circles) and *C. albicans* (pink, triangles). The data points marked with an arrow correspond to the rate constants measured for the yeast enzymes after adjusting the pH of sample solution from 9.5 to neutral.

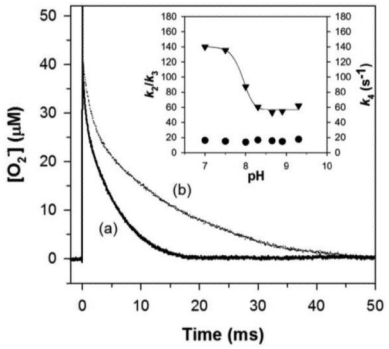

FIGURE 4.

Dependence of the level of product inhibition of *Sc*MnSOD on pH. Decay of 48 μM O_2^- catalyzed by 1 μM (in Mn) *Sc*MnSOD at pH 7.5 (a) and 8.9 (b). Inset: Dependence of the values of k_2/k_3 (circles) and k_4 (triangles) of *Sc*MnSOD on pH. The sample for pulse radiolysis contained 10 mM potassium phosphate (pH 7), 10 mM sodium formate and 10 μM EDTA.

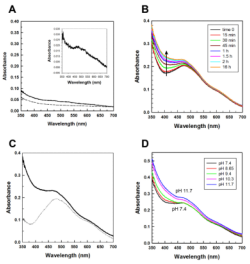

FIGURE 5.

The oxidation state of *Sc*MnSOD. (A) Optical spectra of as-isolated *Sc*MnSOD (solid line) and *Sc*MnSOD reduced by sodium hydrosulfite (dashed line). Inset: The difference spectrum between as-isolated and reduced *Sc*MnSOD. (B) Optical spectra of *Sc*MnSOD oxidized by potassium permanganate ([$KMnO_4$]:MnSOD = 0.75:1) at pH 7.4 as measured over time. Time 0 refers to the start of the first scan immediately after mixing $KMnO_4$ with the enzyme. (C) Reduction of *Sc*Mn^{3+}SOD (solid line, oxidized by 0.75 equiv of $KMnO_4$ and allowed to equilibrate at room temperature for 2 hr) by one equiv of sodium ascorbate (dotted line). (D) Optical spectra of *Sc*Mn^{3+}SOD at different pH. The sample solutions contained 190 μM (in Mn) enzyme in 25 mM potassium phosphate (pH 7.4).

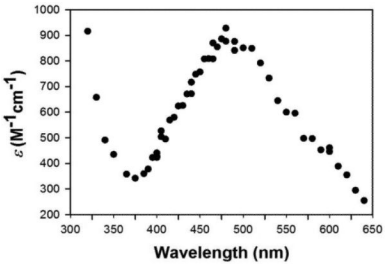

FIGURE 6.

The Mn^{3+}SOD spectrum of *Ca*MnSODc obtained from pulse radiolysis. The pulse radiolysis sample contained 60 μM (in Mn) *Ca*MnSODc in 10 mM potassium phosphate (pH 7), 10 mM sodium formate and 100 μM EDTA. The enzyme was reduced prior to each pulse with 120 μM H_2O_2.

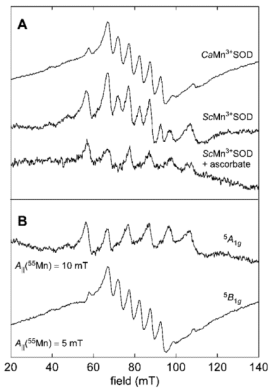

FIGURE 7.

(A) Parallel-mode CW EPR spectrum of *Ca*Mn^{3+}SODc and *Sc*Mn^{3+}SOD oxidized by potassium permanganate ([*Sc*MnSOD]:$KMnO_4$ = 1:0.75) and of *Sc*Mn^{3+}SOD treated with 1 equivalent of sodium ascorbate. (B) The deconvolution of the two spectra (top two spectra in panel A) of the permanganate-oxidized species shows two components, one assigned to a Mn^{3+} center with a $5A_{1g}$ ground state and one with a $5B_{1g}$ ground state. Instrument settings: ν = 9.3959 GHz; microwave power = 32 mW; sweep rate = 1.81 mT/s; temp = 4.9 K.

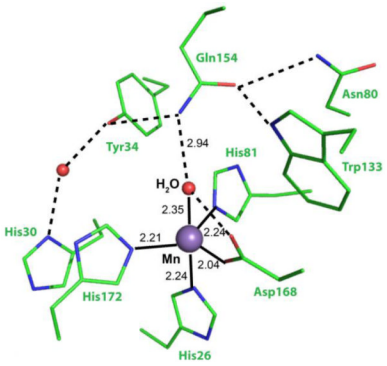

FIGURE 8.

Active site structure of *Sc*MnSOD, showing the coordination sphere of manganese (chain A). Some second coordination sphere residues are also shown. Coordination and hydrogen bonds are indicated as solid and dashed lines, respectively.

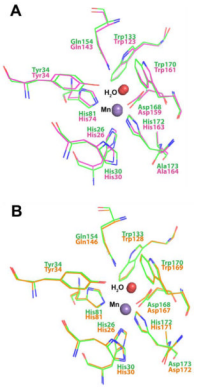

FIGURE 9.
Superposition of the first and second coordination sphere of *Sc*MnSOD to that of human MnSOD (pink, A) and *Ec*MnSOD (yellow, B).

$$M^{n+} + O_2^{-} \rightarrow M^{(n-1)+} + O_2$$

$$M^{(n-1)+} + O_2^{-} + 2H^{+} \rightarrow M^{n+} + H_2O_2$$

Scheme 1.
The Dismutase Mechanism

$$Mn^{3+}SOD + O_2^- \xrightarrow{k_1} Mn^{2+}SOD + O_2 \quad (1)$$

$$Mn^{2+}SOD + O_2^- \xrightarrow{k_2, 2H^+} Mn^{3+}SOD + H_2O_2 \quad (2)$$

$$Mn^{2+}SOD + O_2^- \xrightarrow{k_3} Mn^{3+}(OO^{2-})SOD \quad (3)$$

$$Mn^{3+}(OO^{2-})SOD \xrightarrow{k_4, 2H^+} Mn^{3+}SOD + H_2O_2 \quad (4)$$

Scheme 2.
Catalytic Mechanism of MnSOD

Scheme 3.
Proposed Mechanism of the Reaction of Yeast Mn^{2+}SOD with O_2^-